forests

MDPI

Article

A Study on Spatial Distribution Extraction of Tidal Inundated Mangroves Based on High and Low Tide Level Images

Haotian You [1,2], Qixu You [1], Xu Tang [1], Yao Liu [1], Jianjun Chen [1] and Feng Wang [1,*]

[1] College of Geomatics and Geoinformation, Guilin University of Technology, No. 12 Jian'gan Road, Guilin 541006, China; youht@glut.edu.cn (H.Y.); 2120211909@glut.edu.cn (Q.Y.); 2120211898@glut.edu.cn (X.T.); 1020211833@glut.edu.cn (Y.L.); chenjj@glut.edu.cn (J.C.)

[2] Guangxi Key Laboratory of Spatial Information and Geomatics, Guilin University of Technology, No. 12 Jian'gan Road, Guilin 541004, China

* Correspondence: wangfeng92@glut.edu.cn

Abstract: A majority of mangroves are located in the coastal intertidal zone and are subject to tidal periodic inundation. However, the previous vegetation indices used for extracting the spatial distribution of mangroves were not able to effectively extract submerged mangroves, and the applicability of the vegetation indices used on different spatial resolution images obtained from different sensors was not verified. In this study, a new vegetation index, namely the intertidal mangrove identification indices (*IMII*s), was proposed, based on GF-2 images of high and low tide levels. Meanwhile, other commonly used vegetation indices were also extracted. All the vegetation indices were used to extract the spatial distribution of mangroves under tidal inundation, and applicability tests of the vegetation indices were conducted on Sentinel-2 images in three different regions. It was found that the *IMII*s proposed based on GF-2 images of high and low tide levels can extract submerged mangroves relatively well, and the spatial distribution extraction results of mangroves are better than those of other vegetation indices, with $IMII_2$ outperforming $IMII_1$. At the same time, *IMII*s have good applicability in medium resolution Sentinel-2 images, and there are relatively large differences in the extraction results of mangrove spatial distribution among different vegetation indices in areas with significant impact of tidal inundation. Among all vegetation indices, the extraction results of *IMII*s are relatively superior. In most cases, multi variables collaborative application can improve the accuracy of mangrove spatial distribution extraction results. Based on the results of this study, it was concluded that the *IMII*s proposed in this study can accurately extract the spatial distribution of mangroves inundated by tides from both medium- and high-resolution images, providing accurate basic data for effective management and scientific protection of mangrove resources.

Keywords: mangrove extraction; vegetation indexes; Gaofen-2 images; intertidal mangrove identification index; Sentinel-2 images

Citation: You, H.; You, Q.; Tang, X.; Liu, Y.; Chen, J.; Wang, F. A Study on Spatial Distribution Extraction of Tidal Inundated Mangroves Based on High and Low Tide Level Images. *Forests* **2023**, *14*, 1145. https://doi.org/10.3390/f14061145

Academic Editors: Filiz Bektas Balcik, Fusun Balik Sanli, Fabiana Caló and Antonio Pepe

Received: 19 April 2023
Revised: 26 May 2023
Accepted: 30 May 2023
Published: 1 June 2023

1. Introduction

Mangroves are rare woody plant communities that grow in the transition zone between land and sea [1]. Mangroves are not only economically valuable [2,3] but they also provide a variety of ecological benefits [4,5], such as preventing shoreline erosion [6,7], purifying water, and sequestering carbon [8,9]. However, mangrove resources were seriously threatened due to both natural and human interference, resulting in a sharp decline in the area [3,10,11]. Since 1980, approximately 35% of the world's mangroves disappeared [12]. Global attention was directed at the serious decline in mangrove ecosystems, and the need to protect mangrove resources is urgent [13]. International projects, such as the Ramsar Convention on Wetlands or the Kyoto Protocol, emphasized the importance of taking protective measures and engaging in activities to prevent further loss of mangroves. Accordingly, an accurate assessment of mangrove resources is essential to ensuring a smooth

implementation of the scientific protection of mangrove resources. In addition to predicting disaster-prone areas and providing data support for the formulation of targeted protection policies, this research is highly valuable for identifying disaster-prone areas.

The accurate assessment of the spatial distribution of mangroves is the basis of the monitoring procedure for mangrove resources and also the premise for the effective management and scientific protection of mangrove resources. Although the accuracy of field survey data is high, the unique natural environment of mangroves with its muddy soil and numerous air roots makes it difficult to assess mangroves through the use of traditional mangrove resource survey methods [14]. Moreover, traditional survey methods are time-consuming and difficult to conduct on a large scale. As a result of the emergence of remote sensing technology, it is possible to overcome the shortcomings of traditional investigation methods, and this technology was widely used in investigations conducted on mangrove resources with favorable results. For example, Lorenzo et al. [15] employed Landsat MSS data as a means to monitor the decline of mangrove wetlands in Sanbaoyan, Philippines, in 1979, and were the first to apply remote sensing technology to detect the dynamic changes of mangrove wetlands. Chen et al. [16] conducted a study on the dynamic changes of the spatial distribution of mangroves in Guangxi from 1955 to 2004 through the use of five temporal remote sensing datasets, and they analyzed the factors behind their evolution. Li et al. [17] conducted a study in which they employed a supervised classification, an unsupervised classification, and an object-oriented classification method in order to extract the spatial distribution of mangroves and monitor their dynamic changes based on ALOS PRISM/AVNIR-2 images. Kumar et al. [18] conducted research in which they successfully extracted the spatial distribution of mangroves by employing three classifiers based on five vegetation indexes extracted from EO-1 Hyperion images. The results indicated that support vector machine (SVM) performed the best, with an overall accuracy of 99.08%. Jia et al. [19] conducted research in which they extracted the spatial distribution of mangroves in China from 1973 to 2015 using an object-oriented method and analyzed the dynamic changes of mangroves throughout forty-two years based on one hundred and twenty-three Landsat images. In another study, Jia et al. [20] successfully extracted the vegetation index sensitive to submerged mangroves based on the middle red edge band of Sentinel-2 images. Although a considerable amount of research was conducted on the extraction of the spatial distribution of mangroves based on remote sensing data, there are also certain shortcomings in their approaches that need to be addressed [13]. For example, the impact of different tidal levels is seldom taken into consideration in the extraction of mangrove spatial distribution, and only the remote sensing data of one single tidal level are used, resulting in inaccurate extraction results that lead to inconsistencies between the change monitoring results and the actual observation. Due to the fact that mangroves primarily grow in coastal intertidal zones that are affected by tidal inundation, short mangrove trees may become completely or partially submerged during high tides and may become exposed to water during low tide, resulting in incompletely boundary information of mangroves extracted from remote sensing images at different tide levels [21]. Therefore, for the purpose of accurately extracting the spatial distribution of mangroves, it is necessary to utilize both high and low tide level image data in order to eliminate the impact of tides.

To effectively eliminate the impact of tidal inundation on the extraction results of the spatial distribution of mangroves, researchers tried to extract the mangroves spatial distribution by employing different vegetation indexes. For example, Zhang et al. [22] employed the mangrove recognition index, green vegetation index, and humidity index extracted from the multi-temporal Landsat TM images of different tide levels in order to determine the range and distribution of mangrove trees. According to the results, the user accuracy and producer accuracy of the mangrove trees were 98.09% and 93.19%, respectively. Jia [23] conducted a study based on Landsat remote sensing data, in which he employed the inundated mangrove forest index extracted from Landsat remote sensing data in order to investigate the area, the distribution, and the landscape pattern of the

mangroves in China from 1973 to 2013 using object-oriented and decision tree classification methods. Xu et al. [24] employed the normalized intertidal mangrove index extracted from the Sentinel-2 image of high and low tide levels in order to extract the spatial distribution of mangroves in the intertidal zone, with a user accuracy of 93.98%. The above research results demonstrate that the vegetation index extracted from the high and low tide level image data is capable of improving the extraction accuracy of the spatial distribution results of mangroves, and it can also avoid the impact of tidal inundation on the extraction of the spatial distribution of mangroves in a single-phase image to a certain extent. However, the most vegetation index in the aforementioned studies is calculated based on the visible light band, the short wave infrared band, or the medium wave infrared band of the medium resolution image, which is difficult to directly apply to high-resolution images with relatively few bands.

As a result of current technological advancements, the number of high-resolution remote sensing images available at this stage is increasing and is gradually becoming an essential data source for the extraction of the spatial distribution of mangrove trees. As compared with a medium-resolution remote sensing image, with a high-resolution remote sensing image, it is not only possible to extract the spatial distribution of mangroves in smaller patches, but also the impact of tidal inundation on the spatial distribution of mangroves can be reflected more accurately. However, due to the relatively small number of bands, which usually only contain four bands, namely red, green, blue, and near-infrared, it is difficult to apply the high and low tide vegetation index, which is calculated based on the above short-wave infrared band or medium-wave infrared band. Accordingly, a new vegetation index needs to be extracted from remote sensing images with high resolution in order to identify mangroves that are submerged during tidal cycles. For example, Qing et al. [25] proposed a submerged mangrove recognition index (*SMRI*) based on multi-tidal GF-1 remote sensing images. The *SMRI* only utilized the red and near-infrared bands, and the accuracy of the results was 94%, which was better than the results of single-tide remote sensing images (with an accuracy of 86%). Xia et al. [26] employed the *SMRI* extracted from GF-2 images as a means to map the spatial distribution of mangroves in China, and the overall accuracy was 92% and the *Kappa* coefficient was 0.89. According to the above research results, although the bands of high-resolution images were relatively small, the extraction of vegetation indexes based on multi-tidal high-resolution images was yet capable of achieving better extraction results in the spatial distribution of mangrove trees and can eliminate the impact of tidal inundation to a certain extent. However, the aforementioned high and low tidal vegetation indexes only utilized the red edge and near-infrared bands without taking into account the role of other bands in the extraction of the spatial distribution of mangroves under periodic tidal inundation. For example, in the former studies, it was demonstrated that the green light band is capable of effectively representing the water absorption and greenness of vegetation [27], which may play a certain role in the extraction of inundated mangroves. Similarly, the former studies did not further extend the extraction of vegetation indexes based on high-resolution images to medium-resolution remote sensing images in order to verify that the proposed vegetation index could be applied to the extraction of the spatial distribution of inundated mangroves from medium-resolution remote sensing images.

Accordingly, in this study, a new vegetation index, namely *IMII*s, was proposed based on GF-2 images of high and low tide levels. Additionally, other commonly used vegetation indices were also extracted. All the vegetation indices were used to extract the spatial distribution of mangroves under a tidal inundation, and applicability tests of the vegetation indices were conducted on Sentinel-2 images of three different regions in order to verify the applicability of the vegetation index based on high-resolution images in the case of medium-resolution remote sensing images. This is for the purpose of accurately identifying the spatial distribution of mangroves under tidal inundation in both medium- and high-resolution images simultaneously, as well as providing accurate basic data for effective management and scientific protection of mangrove resources.

2. Materials and Methods

2.1. Study Area

In this study, four different typical mangrove areas located in Guangxi Zhuang Autonomous Region, China, were selected as the study areas, as shown in Figure 1. These areas are from the important mangrove wetlands in China, including two national mangrove nature reserves (Guangxi Beilunhekou National Nature Reserve and Guangxi Shankou Mangrove Ecological Nature Reserve) and one autonomous region nature reserve (Guangxi Maoweihai Autonomous Region Mangrove Nature Reserve). The terrains of these study areas are relatively flat, and there are five main land cover types, including mangroves, terrestrial vegetation (forests, grasslands, and croplands), tidal flats, water (saltwater and freshwater), and built-up land. The regions belong to the subtropical monsoon climate, with an annual average temperature of 21–28 °C and the annual average rainfall of 1713–2823 mm. There is only one tidal rise and fall in one day, also known as a diurnal tide. In the sea area near the Beihai Sea, the maximum tidal range between high and low tide levels can reach 7 m. The mangrove tree species in the research area mainly include Avicennia marina (*Avicennia marina*), Aegiceras corniculatum (*Aegiceras corniculatum* (L) Blanco), Bruguiera gymnorrhiza (*Bruguiera gymnorrhiza* (Linn.) Savigny), Kandelia candel (*Kandelia candel* (Linn) Druce), Excoecaria agallocha (*Excoecaria agallocha* L.), Acanthus ilicifolius (*Acanthus ilicifolius* L.), Rhizophora stylosa (*Rhodophora stylosa* Griff.), and Sonneratia apetala (*Sonneratia apetala* Buch. -Ham.).

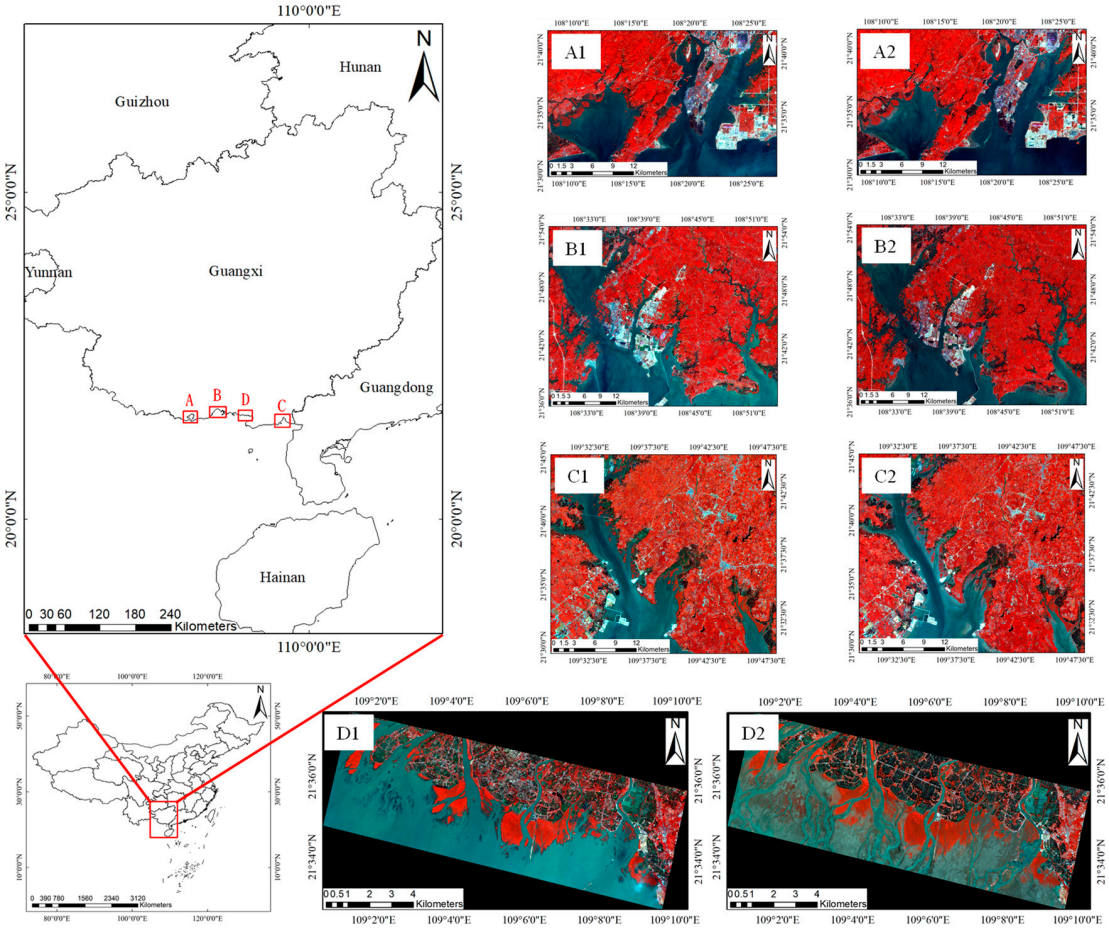

Figure 1. Schematic diagram of the location of the study area; (**A1**) high tide level image of study area A on 9 November 2019; (**A2**) low tide level image of study area A on 28 September 2019; (**B1**) high tide level image of study area B on 9 November 2019; (**B2**) low tide level image of study area B on 28 September 2019; (**C1**) high tide level image of study area C on 20 September 2019; (**C2**) low tide level image of study area C on 30 September 2019; (**D1**) high tide level image of study area D on 7 December 2020; (**D2**) low tide level image of study area D on 27 June 2020.

2.2. Data Introduction and Preprocessing

2.2.1. GF-2 Image

For the purpose of evaluating the potential of extracting the spatial distribution of mangroves in the tidal inundation area based on the vegetation index derived from high-resolution images, the GF-2 image in the study area D shown in Figure 1 was selected for the experiment. The GF-2 satellite was successfully launched on 19 August 2014. It was the first civil optical remote sensing satellite with a spatial resolution less than 1 m, which was independently developed by China. The specific parameters of the sensor are shown in Table 1.

Table 1. The specific parameters of GF-2 satellite sensor.

Bands Number	Spectral Band Range (μm)	Spatial Resolution (m)	Revisit Time (Day)
1	0.45~0.90	0.8	5
2	0.45~0.52	3.2	
3	0.52~0.59		
4	0.63~0.69		
5	0.77~0.89		

According to Table 1, although the revisit period of the GF-2 satellite was 5 days, it was still difficult to obtain high-quality, cloud-free GF-2 image data during high and low tide levels with close dates due to the effects of clouds and rain in coastal areas. To better quantify the impact of tidal inundation on the extraction of the spatial distribution of mangrove trees, the images should be from different tide levels that are as far apart as possible, and the tide level difference should be as large as possible. Based on the above principles, the GF-2 image data of study area D in 2020 were screened, and one image depicting a relatively low tide level (176 cm) on 27 June 2020, and one image depicting a relatively high tide level (274 cm) on 7 December 2020, were selected, as shown in Figure 1(D1,D2). According to this figure, the low mangrove coverage forest was completely submerged as a result of the high tide level.

2.2.2. Sentinel-2 Image

In order to verify the applicability of the high-resolution image extraction index in the case of other medium-resolution images, two Sentinel-2 images of high and low tide levels are selected in the other three regions shown in Figure 1. Sentinel-2 is a multispectral satellite launched by the European Space Agency, as are Sentinel-2A and Sentinel-2B satellites. Sentinel-2A was launched on 23 June 2015, and Sentinel-2B was launched on 7 March 2017. The single satellite revisit period was 10 days, and the double satellite revisit period was 5 days. The main payload is a multispectral imager with a total of 13 bands and a maximum spatial resolution of 10 m. The specific parameters are shown in Table 2.

Both the GF-2 and Sentinel-2 images employed in this study were original image data and, therefore, a series of preprocessing is required, such as radiometric calibration, atmospheric correction, geometric correction, band fusion, resampling, etc. Subsequently, the vegetation index was extracted from the pre-processed image data. All of the above operations were completed through ENVI5.3 and ESA SNAP 8.0 software.

Table 2. The specific parameters of Sentinel-2 satellite sensor.

Bands Number	Central Wavelength (nm)	Resolution (m)	Revisit Period (Day)
Band 1—Coastal aerosol	443.9 (S2A)/442.3 (S2B)	60	
Band 2—Blue	496.6 (S2A)/492.1 (S2B)	10	
Band 3—Green	560 (S2A)/559 (S2B)	10	
Band 4—Red	664.5 (S2A)/665 (S2B)	10	
Band 5—Vegetation Red Edge 1	703.9 (S2A)/703.8 (S2B)	20	
Band 6—Vegetation Red Edge 2	740.2 (S2A)/739.1 (S2B)	20	
Band 7—Vegetation Red Edge 3	782.5 (S2A)/779.7 (S2B)	20	5
Band 8—*NIR*	835.1 (S2A)/833 (S2B)	10	
Band 8A—Vegetation Red Edge	864.8 (S2A)/864 (S2B)	20	
Band 9—Water vapour	1373.5 (S2A)/1376.9 (S2B)	60	
Band 10—SWIR-Cirrus	1373.5 (S2A)/1376.9 (S2B)	60	
Band 11—SWIR-1	1613.7 (S2A)/1610.4 (S2B)	20	
Band 12—SWIR-2	2202.4 (S2A)/2185.7 (S2B)	20	

2.2.3. Sample Data

To more clearly show the differences in the spatial distribution results of mangroves extracted by different vegetation indexes, different land cover types in the study area were combined into three categories, namely mangrove, other vegetation, and non-vegetation. Among them, the mangrove includes high mangrove and low mangrove. Other vegetation includes farmland, forest, and grassland. Additionally, non-vegetation includes building land, tidal flat, water. The detail description of three combined land cover types in the study area are shown in Table 3. The sample data used for land cover classification were randomly selected based on Google Earth high-resolution images, the 2018 China mangrove resources distribution data set, and field survey. The sample number of three combined land cover types in four study areas are shown in Table 4.

Table 3. The detail description of three combined land cover types in the study area.

Land Cover Type		Description
Mangrove	High mangrove	The area covered by mangroves is high and not submerged at high tide
	Low mangrove	The mangrove coverage area is low and submerged during high tide
Other vegetation	Farmland Forest Grassland	Forest, farmland, and grassland coverage area
Non-vegetation	Building land	Building coverage area
	Tidal flat	In the intertidal zone, sand and mud flats are periodically submerged by tides
	Water	Water-covered areas (including oceans and rivers)

Table 4. The sample number of three combined land cover types in four study areas.

Study Area	Number of Images		Number of Samples (Training/Validation)			
	GF-2	Sentinel-2	Mangrove	Other Vegetation	Non-Vegetation	Total
A	0	2	813/840	1105/1149	722/745	2640/2734
B	0	2	498/509	587/616	1002/1023	2087/2148
C	0	2	724/832	896/1070	623/768	2243/2670
D	2	0	1150/1174	521/539	924/956	2595/2669

2.3. Research Method

In order to accurately extract the spatial distribution of mangrove trees under tidal inundation, in this study, the *IMII*s and other commonly used vegetation indices were extracted based on the high and low tide level GF-2 images, respectively, which are used to

extract the mangrove spatial distribution under tidal inundation, and it serves to verify the application potential of the *IMII*s for the extraction of the spatial distribution of mangroves through comparative research. In addition, the above vegetation indices were tested on Sentinel-2 images of three different regions in order to further verify the applicability of the vegetation index based on high-resolution images in the case of medium-resolution remote sensing images, with the aim of achieving the accurate extraction of the spatial distribution of mangroves under tidal inundation from both the medium and high-resolution images at the same time. The technical flow chart used in the study is shown in Figure 2.

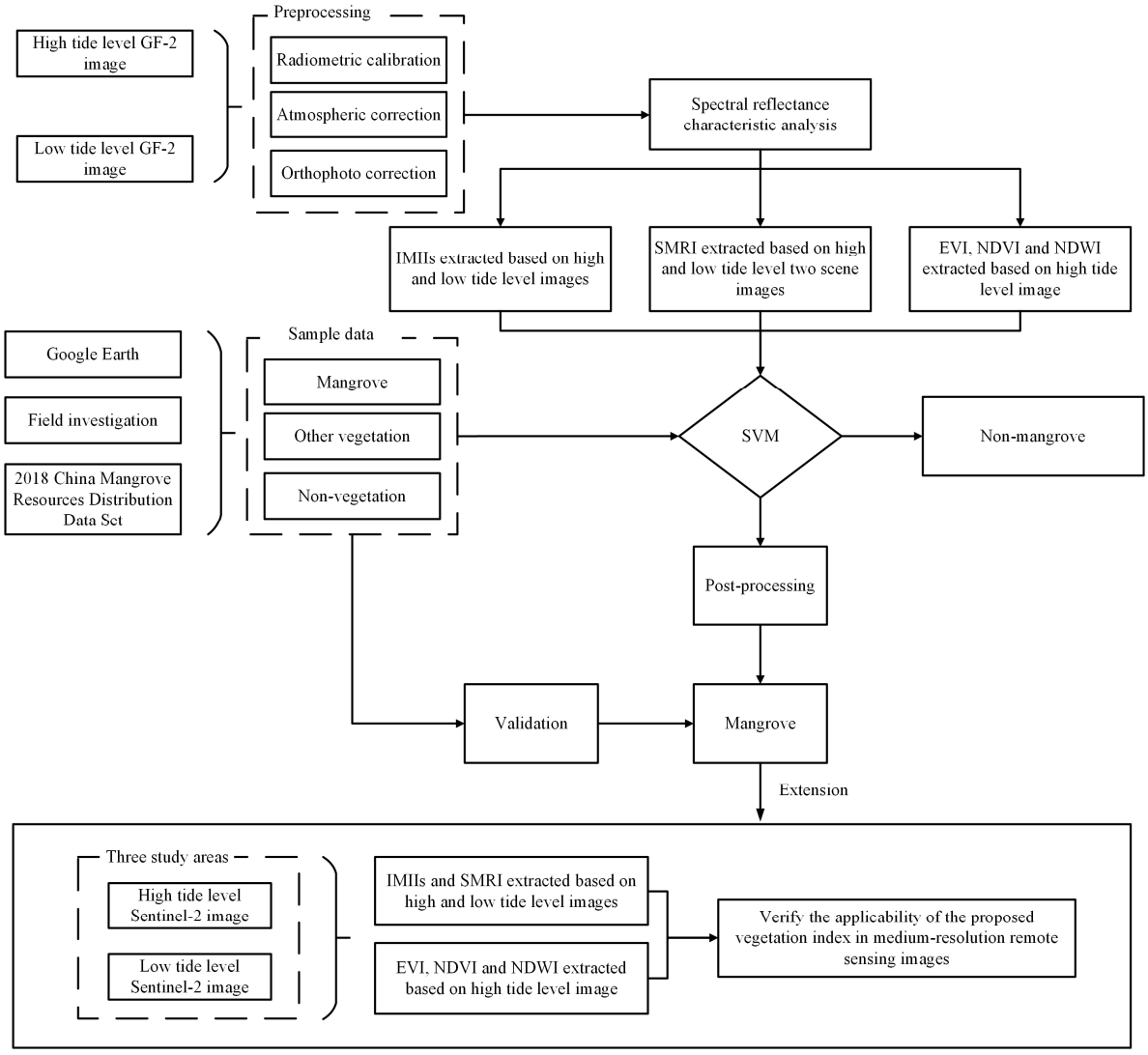

Figure 2. The technical flow chart used in the study.

2.3.1. Proposal of *IMII*

Mangroves are mostly distributed in the coastal intertidal zones. Additionally, the mangroves growing in areas with a lower coverage become periodically submerged by tides. Therefore, in the case of extracting the spatial distribution of mangroves, theoretically using images from lower tide levels can achieve accurate extraction results of the spatial distribution of mangroves growing in lower positions. However, it was difficult to obtain the images at the lowest or highest tide level due to the transit time of satellites, tidal changes, and the influence of clouds and rain. The obtained data were mostly between the highest and lowest tide levels, resulting in mangroves growing in lower positions being more or less submerged, making it difficult to accurately extract the spatial distribution of mangroves.

To achieve accurate extraction of submerged mangroves based on most non-lowest level images, it was attempted to extract new vegetation indices based on high tide level images and the nearest available low tide level images. This can be successfully implemented mainly because the submerged mangroves mostly grow on the edge of mangroves that grow towards the sea, far from humans, and are relatively less affected by human factors. The land cover types do not change completely within several months. However, the nearshore mangroves are greatly affected by humans, and the land cover types may completely change within several months, resulting in the extraction of nearshore mangroves based on low tide images with several months difference not being consistent with the latest actual situation. The spectral reflectance curves of different land cover types based on GF-2 images at high and low tide levels were analyzed, as shown in Figure 3. According to Figure 3, the trend of reflectance curves of tidal-flats, farmland, water, and mangroves growing in higher positions are basically consistent at high and low tide levels, while the mangroves growing in lower positions exhibited significant separation in the case of the near infrared band.

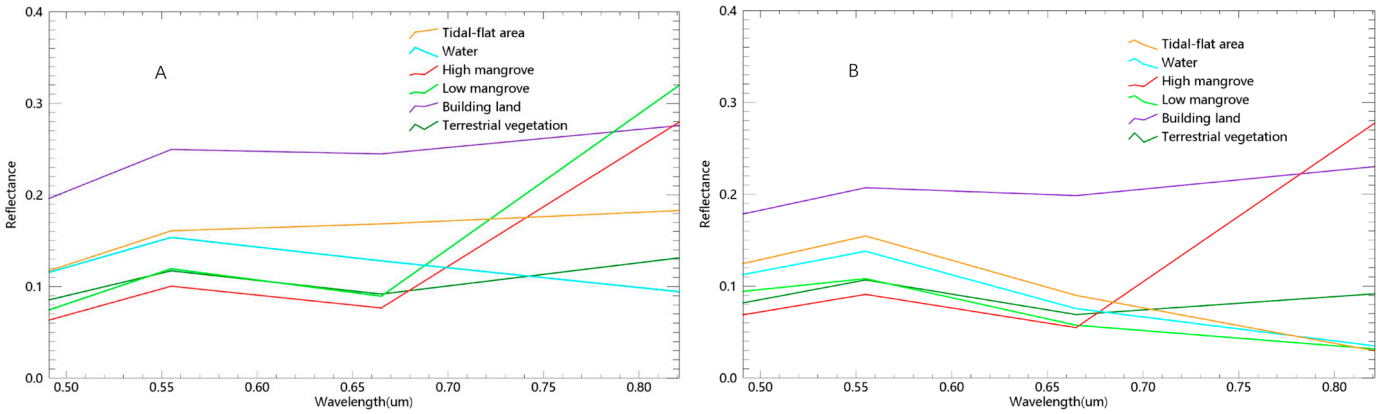

Figure 3. Spectral reflectance curve of different land cover types based on GF-2 images at different tide levels: (**A**) Low tide level; (**B**) High tide level.

At high tide, mangroves growing in lower positions become submerged by seawater. The spectral characteristics of mangroves in lower positions not only include those of seawater, but also those of underwater mangroves. Based on the results depicted in Figure 3, it became apparent that there existed a noticeable spectral resemblance among water, tidal-flats, and mangroves in lower positions. Notably, during both low and high tides, distinct discrepancies can be observed in the spectral characteristics of mangroves in lower positions and tidal-flats within the near-infrared wavelength range. In comparison to bands 1–3, the *NIR* band demonstrated a heightened sensitivity towards both vegetation and water content.

Although water typically absorbed almost all reflected signals in the near-infrared spectrum, the spectral reflectance of seawater in the near-infrared band was not zero, due to factors such as sediment and inundation of mangroves, as shown in Figure 3. At the same time, in the submerged mangrove area, the seawater will absorb and scatter some energy of the green band, resulting in a lower green spectral reflectance of the submerged mangrove, while the vegetation that was not submerged had a higher green spectral reflectance. The spectral reflectance characteristics of the blue band between submerged mangroves and water were similar, but there were still some differences. Specifically, the water had a higher spectral reflectance in the blue band, while in the submerged mangrove areas, due to the coexistence of water and vegetation, the reflectance in the blue band was relatively lower. Additionally, pigments were also the main factor affecting the spectral response of visible light in vegetation, with chlorophyll playing an important role [28]. The chlorophyll absorption peak appeared in the blue and red bands, and the reflection peak appeared in the green band. Chlorophyll and cellulose were transparent to the near-infrared wavelength, and

leaves exhibited a lesser degree of absorption; thus, most of the light beams were transmitted and reflected [29]. The green band is capable of representing the water absorption and greenness of vegetation accurately [27]. Compared with bands 1, 2, and 4, the green band was more sensitive to changes in the water content of the vegetation canopy.

Based on the spectral reflectance characteristics of different bands and the differences in spectral reflectance of different land cover types at high and low tide levels, the new vegetation indices were proposed based on GF-2 images of high and low tide levels, namely the Intertidal Mangrove Identification Index (*IMII*), to extract the spatial distribution of mangroves, as shown in Formula (1).

$$IMII_1 = \frac{NIR_l - Green_h}{NIR_l + Green_h} * \frac{Green_l}{Blue_l} \quad (1)$$

In the equation, $IMII_1$ is the intertidal mangrove identification index; NIR_l is the spectral reflectance value of *NIR* band at low tide level; $Green_h$ is the spectral reflectance value of green band at high tide level; $Green_l$ is the spectral reflectance value of green band at low tide level; and $Blue_l$ is the spectral reflectance value of blue band at low tide level.

From Formula (1), it can be seen that the influence of red bands was not considered in $IMII_1$. In order to further explore the impact of red bands on the extraction results, another new vegetation index, $IMII_2$, was proposed based on Formula (1) by introducing the red band, as shown in Formula (2).

$$IMII_2 = \frac{NIR_h - Red_h}{NIR_h + Red_h} * \frac{NIR_l - Green_h}{NIR_l + Green_h} * \frac{Green_l}{Blue_l} \quad (2)$$

In the equation, NIR_h is the spectral reflectance value of *NIR* band at high tide level; Additionally, Red_h is the spectral reflectance value of Red band at high tide level.

2.3.2. Other Common Vegetation Indexes

As a means of evaluating the capability of the *IMII* to extract spatial distributions of mangroves, other commonly used vegetation indexes were extracted, mainly including *NDVI*, normalized difference water index (*NDWI*), enhanced vegetation index (*EVI*) and *SMRI*. Among them, *NDVI* and *EVI* are the most commonly used greenness indexes for measuring the health and the greenness of vegetation [30,31]. *NDWI* is capable of highlighting water body data in images for the purpose of studying the water content of vegetation [32]. *SMRI* is the existing vegetation indexes specially used for mangrove extraction [33]. The specific calculation formula for each vegetation index is shown in Equations (3)–(6).

$$NDVI = \frac{NIR - Red}{NIR + Red} \quad (3)$$

$$NDWI = \frac{Green - NIR}{Green + NIR} \quad (4)$$

$$EVI = 2.5 \times \frac{NIR - Red}{NIR + 6 \times Red - 7.5 \times Blue + 1} \quad (5)$$

$$SMRI = (NDVI_l - NDVI_h) * \frac{NIR_l - NIR_h}{NIR_h} \quad (6)$$

In the equation, *Green* and *NIR* are the reflectance values of green and near infrared bands, *Red* and *Blue* are the reflectance values of red and blue bands, $NDVI_l$ and $NDVI_h$ are the *NDVI* values of low tide and high tide, and NIR_l and NIR_h are the reflectance values of low tide and high tide near infrared bands, respectively.

2.3.3. Algorithm for Extracting Spatial Distribution of Mangroves

In this paper, support vector machine (SVM) algorithm was employed to extract the spatial distribution of mangroves. To study the differences in the extraction results of spatial distribution of submerged mangroves using different vegetation indices, each of the vegetation indices was first used as input variable for SVM algorithm. Then, on the basis of the single variable extraction results, multiple variables were synergistically applied to improve the accuracy of the spatial distribution extraction results of submerged mangroves. SVM is a variety of generalized linear classifier that classifies data in a binary way according to supervised learning. The decision boundary was determined by the maximum margin hyperplane to solve the learning sample [34–36], as shown in Figure 4.

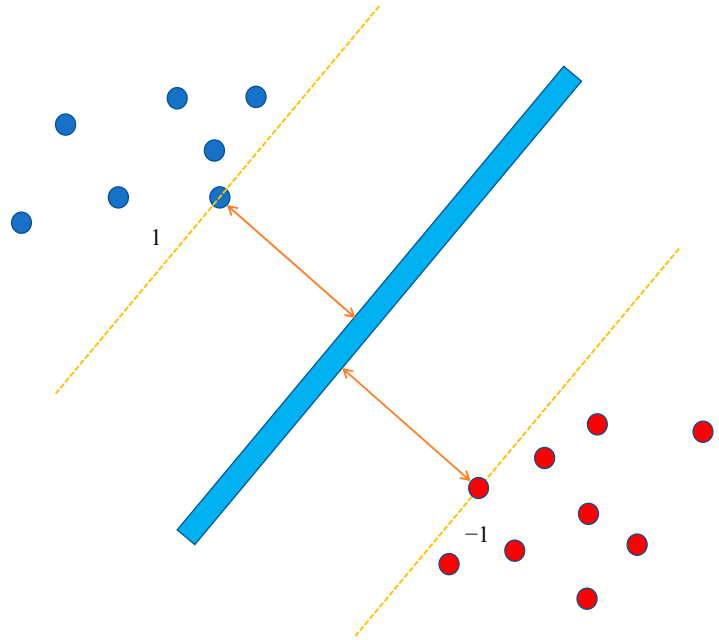

Figure 4. Linear separation of SVM.

In cases where the subject was linearly non-separable, such as in data mixing, nonlinear functions were utilized as a means to map the nonlinear separable problem from the original feature space to the higher-dimensional Hilbert space, and it was then converted into a linear separable problem. In this stage, the hyperplane of the decision boundary is shown in Equation (7).

$$\omega^T \phi(X) + b = 0 \tag{7}$$

where X is the mapping function; however, it is too complex to perform a series of calculations such as the inner product at this time; thus, the kernel function is employed, i.e., the inner product of the mapping function is defined as the kernel function, as shown in Equation (8).

$$k(X_1, X_2) = \phi(X_1)^T \phi(X_2) \tag{8}$$

In this study, the commonly used radial basis function kernel is selected, as shown in Equation (9).

$$k(X_1, X_2) = \exp\left(-\frac{\|X_1 - X_2\|^2}{2\sigma^2}\right) \tag{9}$$

2.3.4. Accuracy Evaluation

To evaluate the accuracy of mangrove classification results, the sample data obtained from Google high-resolution images, field surveys, and the 2018 mangrove dataset (as shown in Table S4) included two parts with about 1:1 ratio. The training part was used to

establish the mangrove classification models and the validation part was used to evaluate the accuracy of model classification results. The accuracy evaluation indicators mainly included user accuracy (*UA*), producer accuracy (*PA*), overall accuracy (*OA*), and *Kappa* coefficient (*K*). The calculation formulas are as shown in Equations (10)–(13).

$$UA_i = \frac{p_{ii}}{p_{i+}} \tag{10}$$

$$PA_i = \frac{p_{ii}}{p_{+i}} \tag{11}$$

$$OA = \frac{p\sum_{i=1}^{k} p_{ii}}{p} \tag{12}$$

$$kappa = \frac{p\sum_{i=1}^{k} p_{ii} - \sum_{i=1}^{k} p_{i+}p_{+i}}{p^2 - \sum_{i=1}^{k} p_{i+}p_{+i}} \tag{13}$$

where p is the total number of samples; K is the total number of categories; P_{ii} is the number of samples correctly classified; P_{+i} is the number of samples in category i; P_{i+} is the number of samples predicted for category i.

3. Results and Analysis

3.1. Results of Mangroves Spatial Distribution Extraction Based on GF-2 Images with Different Vegetation Indices

Based on the GF-2 image, *IMII* and other commonly used vegetation indexes were used to extract the spatial distribution of mangroves. The results are shown in Figure 5, and the accuracy evaluation results are shown in Table 5. The corresponding high-resolution image from Google Earth can be found in Figure S4 in the Supplementary Materials.

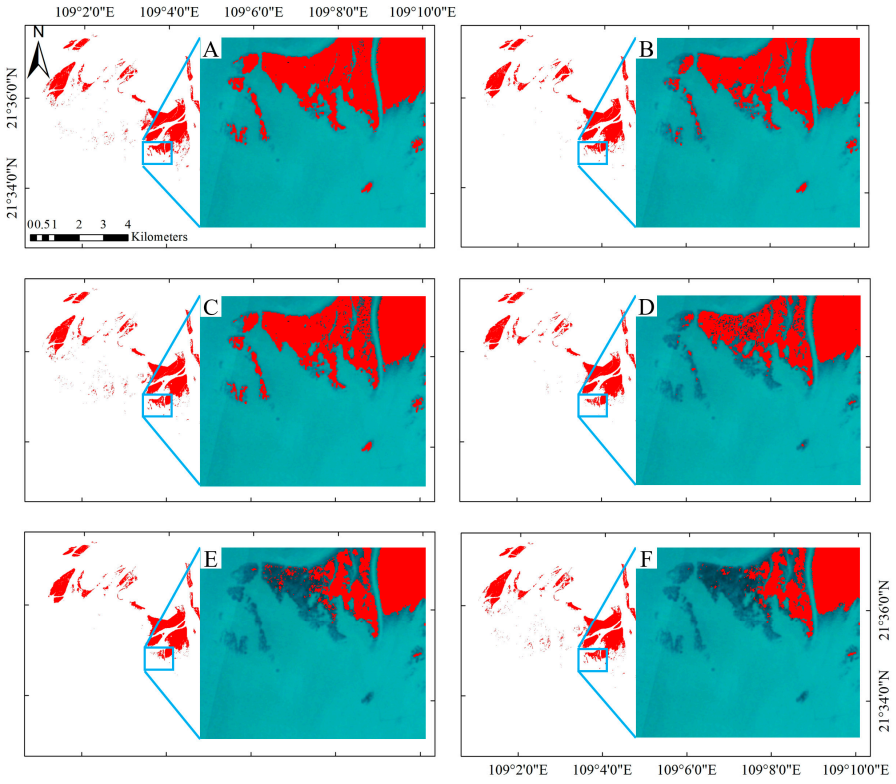

Figure 5. Results of the spatial distribution extraction of mangroves with different vegetation indices based on GF-2 images: (**A**) $IMII_1$; (**B**) $IMII_2$; (**C**) *SMRI*; (**D**) *EVI*; (**E**) *NDVI*; (**F**) *NDWI*.

Table 5. Accuracy evaluation of the extraction results of the spatial distribution of mangroves with different vegetation indexes based on GF-2 images.

Vegetation Indexes	Classification Results			Vegetation Indexes	Classification Results		
		PA	*UA*			*PA*	*UA*
***IMII*$_1$**	Mangrove	94.04%	96.00%	***IMII*$_2$**	Mangrove	95.49%	96.14%
	Non-Mangrove	89.40%	86.47%		Non-Mangrove	88.08%	86.93%
	OA	91.49%			*OA*	91.79%	
	Kappa	0.8677			*Kappa*	0.8717	
		PA	*UA*			*PA*	*UA*
SMRI	Mangrove	90.46%	96.11%	***EVI***	Mangrove	87.73%	95.72%
	Non-Mangrove	86.39%	80.97%		Non-Mangrove	86.77%	79.95%
	OA	88.19%			*OA*	87.30%	
	Kappa	0.8178			*Kappa*	0.8039	
		PA	*UA*			*PA*	*UA*
NDVI	Mangrove	87.22%	95.43%	***NDWI***	Mangrove	88.42%	96.20%
	Non-Mangrove	87.12%	79.98%		Non-Mangrove	87.19%	80.27%
	OA	87.15%			*OA*	87.64%	
	Kappa	0.8019			*Kappa*	0.8095	

According to the results shown in Figure 5, it was not possible to accurately extract the submerged mangroves by employing the *EVI*, *NDVI*, and *NDWI* indexes proposed based on the single tide image. In particular, in cases where the tide level was high, a large number of mangroves in the flooded area became undetectable, as shown in the partially enlarged areas of Figure 5D–F. While the extraction results of *IMII*$_1$, *IMII*$_2$ and *SMRI* based on the high and low tide level images were more accurate, this made it possible to distinguish the submerged mangroves in the case of a high tide level, as shown in the partially enlarged areas of Figure 5A–C. Additionally, the extraction result of the *IMII*$_2$ was more accurate than that of the *IMII*$_1$ and *SMRI*, due to the fact that the *IMII*$_1$ and *SMRI* failed to effectively extract the submerged mangroves in some areas.

According to Table 5, it was indicated that the spatial distribution extraction of mangroves based on the vegetation index extracted from GF-2 images achieved accurate results, with an overall accuracy of more than 87% and a *Kappa* coefficient higher than 0.80. Among them, the result of *IMII*$_2$ was the best, with an overall accuracy and a *Kappa* coefficient of 91.79% and 0.87, respectively. Next, the results of *IMII*$_1$ included an overall accuracy and *Kappa* coefficient of 91.49% and 0.87, respectively. While the results of *NDVI* were the lowest, with an overall accuracy and *Kappa* coefficient of 87.15% and 0.80, respectively.

Meanwhile, the user accuracy of the mangrove extraction results with *EVI*, *NDVI*, and *NDWI* was high; however, the mapping accuracy was low, which indicates that there were many errors in the mangrove spatial distribution extraction results. This is relatively consistent with the results shown in Figure 5, i.e., the above four vegetation indexes were unable to effectively extract the submerged mangroves, and the spatial distribution of the mangroves became significantly underestimated in the case where the high tide remote sensing image was employed to extract the mangrove trees. On the contrary, *IMII*s and *SMRI* were capable of effectively distinguishing submerged mangroves in the case of extracting mangroves from high tide remote sensing images, and the extraction result of *IMII*$_2$ was superior to the result of *IMII*$_1$. Therefore, the difference between the user accuracy and mapping accuracy of *IMII*$_1$ and *IMII*$_2$ was small, and in the case of *IMII*$_2$, the difference was smaller, with results of 0.65% less than the difference of *IMII*$_1$ at 1.96%.

Based on the results of univariate, the extraction of the spatial distribution of mangroves through multivariate collaboration was attempted, and the results are shown in Table 6. Due to the large number of multivariate combination classification results, it was not convenient to display them all. Therefore, only some of the multivariate combination classification results are shown in Table 6. And the confusion matrices of land cover classi-

fication with some vegetation indices based on GF-2 images can be found in Table S1 in the Supplementary Materials.

Table 6. Partial multivariate combination classification results.

Multivariable Combination	Classification Results			Multivariable Combination	Classification Results		
		PA	*UA*			*PA*	*UA*
IMII*$_1$, *NDWI	Mangrove	95.91%	98.00%	***IMII*$_2$, *NDWI***	Mangrove	92.33%	94.26%
	Non-Mangrove	91.07%	88.22%		Non-Mangrove	84.33%	81.59%
	OA	93.26%			*OA*	88.12%	
	Kappa	0.8949			*Kappa*	0.8155	
		PA	*UA*			*PA*	*UA*
SMRI, NDVI	Mangrove	95.74%	96.56%	***EVI, NDVI***	Mangrove	86.63%	94.96%
	Non-Mangrove	85.92%	83.61%		Non-Mangrove	86.31%	79.20%
	OA	90.18%			*OA*	86.51%	
	Kappa	0.8476			*Kappa*	0.7922	
		PA	*UA*			*PA*	*UA*
IMII*$_1$, *NDWI*, *NDVI	Mangrove	94.38%	97.97%	***SMRI, NDWI, NDVI***	Mangrove	95.14%	98.24%
	Non-Mangrove	91.83%	87.69%		Non-Mangrove	88.34%	84.24%
	OA	92.92%			*OA*	91.05%	
	Kappa	0.89			*Kappa*	0.8614	

Analyzing the results presented in Tables 5 and 6, it can be observed that, in most cases, the accuracy of multivariate collaborative applications was superior to those of univariate. For bivariate classification results shown in Table 6, the result based on *IMII*$_1$ and *NDWI* was the best, with an overall accuracy of 93.26% and a *Kappa* coefficient of 0.8949, which was superior to all univariate classification results. For the three-variable classification results, although the result based on the combination of *IMII*$_1$, *NDWI*, and *NDVI* variables outperformed the univariate classification results, it was lower than the classification results of *IMII*$_1$ and *NDWI*. The results indicate that although multivariable collaborative applications can improve classification results to a certain extent in most cases, inappropriate variable combinations not only fail to improve the classification results, but also reduce the classification results.

In summary, the vegetation index extracted based on GF-2 images allowed for the extraction of more accurate spatial distribution results for mangroves. Furthermore, the *IMII*$_1$ and *IMII*$_2$ derived from high and low tide level images were capable of effectively extracting submerged mangroves, and the results were also more accurate than those of other vegetation indexes, while the extraction result of *IMII*$_2$ was the best. Although multivariable collaborative applications can improve classification results in most cases, it is important to pay attention when applying multivariable collaboration, as inappropriate variable combinations not only fail to improve classification results, but also lower classification results.

3.2. Results of Mangrove Spatial Distribution Extraction Based on Senitnel-2 Images with Different Vegetation Indices

For further verification of the applicability of the extraction of vegetation indices based on GF-2 images for medium-resolution images, the proposed vegetation index was tested on Sentinel-2 images of three regions within study areas A, B, and C. And the high-resolution images from Google Earth in study areas A, B, and C can be found in Figures S1, S2 and S3 in the Supplementary Materials. The extraction results for the spatial distribution of mangroves in study area D are shown in Figure 6, and the precision evaluation results are shown in Table 7.

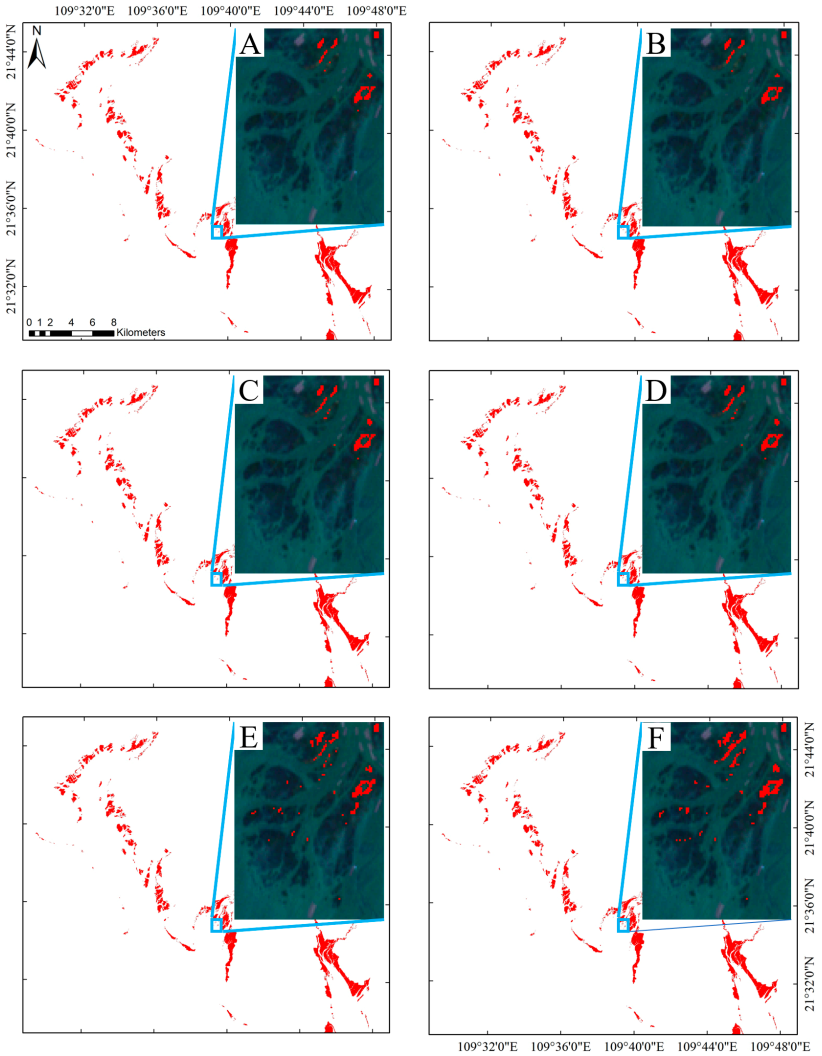

Figure 6. Results of mangroves spatial distribution extraction with different vegetation indices based on Sentinel-2 images in study area A: (**A**) $IMII_1$; (**B**) $IMII_2$; (**C**) *SMRI*; (**D**) *EVI*; (**E**) *NDVI*; (**F**) *NDWI*.

Table 7. Accuracy evaluation of the extraction results of the spatial distribution of mangroves with different vegetation indexes based on Sentinel-2 images in study area A.

Vegetation Indexes	Classification Results			Vegetation Indexes	Classification Results		
		PA	*UA*			*PA*	*UA*
***IMII*$_1$**	Mangrove	95.24%	91.32%	***IMII*$_2$**	Mangrove	96.67%	90.83%
	Non-Mangrove	87.35%	82.17%		Non-Mangrove	87.77%	92.48%
	OA	90.64%			*OA*	91.11%	
	Kappa	0.8558			*Kappa*	0.8636	
		PA	*UA*			*PA*	*UA*
SMRI	Mangrove	95.00%	89.26%	***EVI***	Mangrove	95.96%	87.58%
	Non-Mangrove	86.43%	92.26%		Non-Mangrove	88.89%	92.50%
	OA	89.87			*OA*	89.60%	
	Kappa	0.8441			*Kappa*	0.8413	
		PA	*UA*			*PA*	*UA*
NDVI	Mangrove	96.31%	85.29%	***NDWI***	Mangrove	96.66%	85.08%
	Non-Mangrove	87.95%	94.46%		Non-Mangrove	84.37%	92.55%
	OA	90.49%			*OA*	88.64%	
	Kappa	0.8556			*Kappa*	0.8269	

According to the results shown in Figure 6, in the case of the Sentinel-2 image, while the overall difference between the extraction results of the spatial distribution of mangroves based on the vegetation index was not obvious, the difference became apparent in the case of certain distinct areas, as shown in the partially enlarged area in Figure 6. According to the partially enlarged area in Figure 6, it can be observed that in this particular area, the extraction areas for $IMII_1$, $IMII_2$, *SMRI*, and *EVI* were relatively smaller, while *NDVI*, and *NDWI* exhibited larger extraction areas for mangroves. This was primarily due to the severe invasion of *Spartina alterniflora* Loisel. in this region. *NDVI* and *NDWI* tended to misclassify *Spartina alterniflora* Loisel. as mangroves, to some extent, during the mangrove extraction process, resulting in a larger extracted area for mangroves. On the other hand, other indices are better at distinguishing between mangroves and *Spartina alterniflora* Loisel., leading to a relatively smaller extracted area for mangroves.

According to Table 7, the extraction results of the spatial distribution of mangroves based on the vegetation index extracted from the Sentinel-2 image in study area A were accurate enough and the difference was not obvious. The overall accuracy was higher than 88%, and the *Kappa* coefficient was greater than 0.8. Among them, the overall accuracy and *Kappa* coefficient of $IMII_2$ were the highest, with 91.11% and 0.86, respectively, followed by $IMII_1$, where the overall accuracy and *Kappa* coefficient were 90.64% and 0.86, respectively. The results of the *NDWI* were the lowest, with an overall accuracy and *Kappa* coefficient of 88.64% and 0.83, respectively.

Meanwhile, the mapping accuracy of mangrove extraction results for each vegetation index was high; however, the user accuracy was low, which indicates that there were many missing errors in the extraction results of the spatial distribution of mangrove trees. The difference between the user accuracy and the mapping accuracy of $IMII_1$ was the smallest, with only 3.92%, while the difference between the user accuracy and the mapping accuracy of *NDWI* was the largest, at 11.58%. Several factors contributed to this situation, including the complex and scattered nature of the mangrove tree species in the region and the invasion of *Spartina alterniflora* Loisel., particularly in the Dandouhai region, which causes *Spartina alterniflora* Loisel. to be divided into mangrove forests in the majority of cases.

Furthermore, the spatial distribution of mangroves was also extracted through multivariate collaboration in study area A, and the results are shown in Table 8. And the confusion matrices of land cover classification with some vegetation indices based on Sentinel-2 images in study area A can be found in Table S2 in the Supplementary Materials.

Table 8. Partial multivariate combination classification results.

Multivariable Combination	Classification Results			Multivariable Combination	Classification Results		
		PA	*UA*			*PA*	*UA*
$IMII_1$, NDWI	Mangrove	96.31%	91.00%	***$IMII_2$, NDWI***	Mangrove	96.43%	90.91%
	Non-Mangrove	87.07%	92.25%		Non-Mangrove	88.04%	92.53%
	OA	90.71%			*OA*	91.19%	
	Kappa	0.8571			*Kappa*	0.8647	
		PA	*UA*			*PA*	*UA*
SMRI, NDVI	Mangrove	96.07%	87.15%	***EVI, NDVI***	Mangrove	96.07%	87.06%
	Non-Mangrove	90.13%	95.05%		Non-Mangrove	89.60%	94.36%
	OA	91.84%			*OA*	91.44%	
	Kappa	0.8755			*Kappa*	0.8694	
		PA	*UA*			*PA*	*UA*
$IMII_1$, NDWI, NDVI	Mangrove	96.31%	90.29%	***SMRI, NDWI, NDVI***	Mangrove	93.07%	87.91%
	Non-Mangrove	89.60%	93.97%		Non-Mangrove	90.81%	95.37%
	OA	92.03%			*OA*	92.36%	
	Kappa	0.8778			*Kappa*	0.8833	

According to the results presented in Tables 7 and 8, it can be observed that the accuracy of multivariate collaborative applications was superior to those of univariate. For bivariate classification results shown in Table 8, the result based on *SMRI* and *NDVI* was the best, with an overall accuracy of 91.84% and a *Kappa* coefficient of 0.8755, which was superior to all univariate classification results. For the three-variable classification results, the result based on the combination of *SMRI*, *NDWI*, and *NDVI* variables outperformed the bivariate and univariate classification results. The results indicate that for study area A, although multivariate collaborative application can improve classification results, the improvement was relatively small.

The extraction results of the spatial distribution of mangroves with each vegetation index based on Sentinel-2 images in study area B are shown in Figure 7, and the accuracy evaluation results are shown in Table 9.

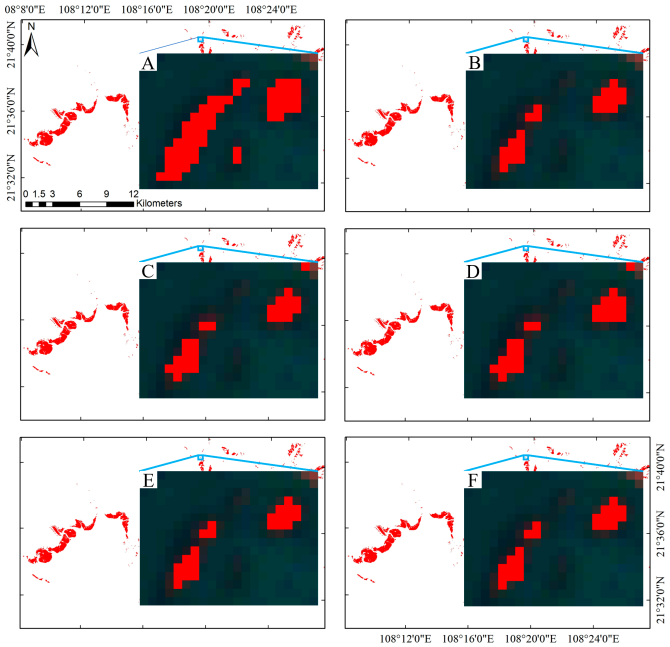

Figure 7. Results of mangroves spatial distribution extraction with different vegetation indices based on Sentinel-2 images in study area B: (**A**) $IMII_1$; (**B**) $IMII_2$; (**C**) *SMRI*; (**D**) *EVI*; (**E**) *NDVI*; (**F**) *NDWI*.

Table 9. Accuracy evaluation of the extraction results of the spatial distribution of mangroves with different vegetation indexes based on Sentinel-2 images in study area B.

Vegetation Indexes	Classification Results			Vegetation Indexes	Classification Results		
		PA	*UA*			*PA*	*UA*
***IMII*$_1$**	Mangrove	97.25%	99.20%	***IMII*$_2$**	Mangrove	97.25%	99.00%
	Non-Mangrove	89.90%	89.49%		Non-Mangrove	89.86%	89.56%
	OA	92.27%			*OA*	92.27%	
	Kappa	0.8780			*Kappa*	0.8780	
		PA	*UA*			*PA*	*UA*
SMRI	Mangrove	97.45%	99.20%	***EVI***	Mangrove	97.45%	99.20%
	Non-Mangrove	89.75%	89.34%		Non-Mangrove	89.73%	89.33%
	OA	92.18%			*OA*	92.18%	
	Kappa	0.8766			*Kappa*	0.8765	
		PA	*UA*			*PA*	*UA*
NDVI	Mangrove	97.64%	98.22%	***NDWI***	Mangrove	97.84%	98.61%
	Non-Mangrove	89.17%	89.18%		Non-Mangrove	88.92%	88.64%
	OA	91.90%			*OA*	91.62%	
	Kappa	0.8721			*Kappa*	0.8679	

According to Figure 7, the overall and detailed differences in the extraction results of the spatial distribution of mangroves with each vegetation index were not obvious. This was mainly because the mangroves in this area were relatively tall and, therefore, less affected by tidal inundation. In most areas, mangrove areas that were affected by tidal inundation were smaller than 10 m, while the spatial resolution of Sentinel-2 images was 10 m, thus making it difficult to reach a complete pixel. The effect of the tidal inundations on the spatial distribution of mangroves was less than one pixel; hence, the difference in the spatial distribution of mangroves extracted through different vegetation indexes was not significant.

According to Table 9, the spatial distribution extraction results of mangroves based on the vegetation index extracted from Sentinel-2 images in study area B were accurate enough and the difference was not obvious. The overall accuracy was higher than 91.6%, and the *Kappa* coefficient was greater than 0.86. Among them, the overall accuracy and *Kappa* coefficient of *IMII*s were the highest, at 92.27% and 0.88, respectively. The results of *NDWI* were the lowest, and the overall accuracy and *Kappa* coefficient were 91.62% and 0.87, respectively, which were only 0.65% different from the results of *IMII*s.

Meanwhile, the extraction results of the spatial distribution of mangroves with each vegetation index were accurate, and there were no significant errors either. In addition, the user accuracy and mapping accuracy of the extraction results for each vegetation index were high. This was mainly due to the fact that the mangrove trees in this area were relatively tall, and the image depicting tidal inundation was relatively small.

At the same time, the spatial distribution of mangroves was also extracted through multivariate collaboration in study area B, and the specific results are shown in Table 10. And the confusion matrices of land cover classification with some vegetation indices based on Sentinel-2 images in study area B can be found in Table S3 in the Supplementary Materials.

Table 10. Partial multivariate combination classification results.

Multivariable Combination	Classification Results			Multivariable Combination	Classification Results		
		PA	*UA*			*PA*	*UA*
IMII*$_1$, *NDWI	Mangrove	97.84%	98.81%	***IMII*$_2$, *NDWI***	Mangrove	97.84%	99.01%
	Non-Mangrove	88.84%	88.47%		Non-Mangrove	89.19%	88.83%
	OA	91.53%			*OA*	91.81%	
	Kappa	0.8665			*Kappa*	0.8709	
		PA	*UA*			*PA*	*UA*
SMRI*, *NDVI	Mangrove	97.64%	98.22%	***EVI*, *NDVI***	Mangrove	97.64%	98.22%
	Non-Mangrove	88.93%	88.82%		Non-Mangrove	88.84%	88.68%
	OA	91.67%			*OA*	91.57%	
	Kappa	0.8686			*Kappa*	0.8672	
		PA	*UA*			*PA*	*UA*
IMII*$_1$, *NDWI*, *NDVI	Mangrove	98.04%	99.01%	***SMRI*, *NDWI*, *NDVI***	Mangrove	97.64%	98.61%
	Non-Mangrove	89.26%	89.01%		Non-Mangrove	89.00%	88.70%
	OA	91.95%			*OA*	91.67%	
	Kappa	0.8730			*Kappa*	0.8687	

Based on the results shown in Tables 9 and 10, it can be observed that for study area B, the multivariate collaborative application did not improve the accuracy of classification results. Compared with the results of univariate classification, the results of multivariate collaborative applications showed a decrease. This was mainly because in the study area B, the impact of tidal inundation on mangroves was relatively small, and univariate can achieve more accurate extraction of mangrove spatial distribution, while the multivariate collaborative application actually reduced the classification results.

The extraction results of the spatial distribution of mangroves with each vegetation index based on Sentinel-2 images in study area C are shown in Figure 8, and the accuracy evaluation results are shown in Table 11.

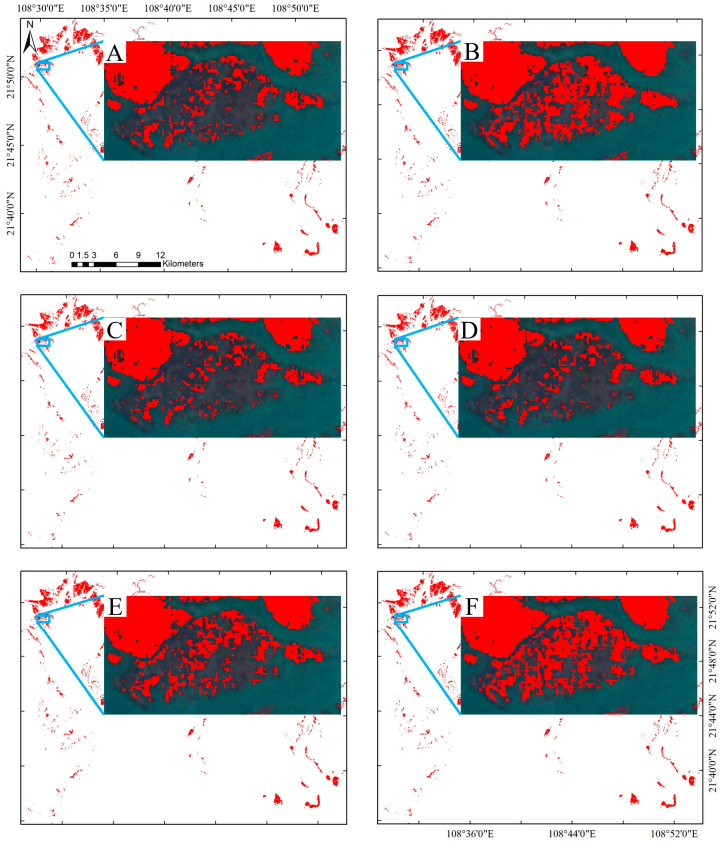

Figure 8. Results of mangroves spatial distribution extraction with different vegetation indices based on Sentinel-2 images in study area C: (**A**) $IMII_1$; (**B**) $IMII_2$; (**C**) *SMRI*; (**D**) *EVI*; (**E**) *NDVI*; (**F**) *NDWI*.

Table 11. Accuracy evaluation of the extraction results of the spatial distribution of mangroves with different vegetation indexes based on Sentinel-2 images in study area C.

Vegetation Indexes	Classification Results			Vegetation Indexes	Classification Results		
		PA	*UA*			*PA*	*UA*
***IMII*$_1$**	Mangrove	95.91%	88.47%	***IMII*$_2$**	Mangrove	95.91%	92.36%
	Non-Mangrove	91.71%	95.12%		Non-Mangrove	93.31%	95.10%
	OA	92.66%			*OA*	93.97%	
	Kappa	0.889			*Kappa*	0.9086	
		PA	*UA*			*PA*	*UA*
SMRI	Mangrove	95.91%	88.96%	***EVI***	Mangrove	95.91%	88.96%
	Non-Mangrove	91.92%	95.06%		Non-Mangrove	91.92%	95.06%
	OA	92.81%			*OA*	92.81%	
	Kappa	0.8912			*Kappa*	0.8912	
		PA	*UA*			*PA*	*UA*
NDVI	Mangrove	95.43%	88.42%	***NDWI***	Mangrove	95.67%	89.64%
	Non-Mangrove	91.98%	95.03%		Non-Mangrove	92.49%	95.20%
	OA	92.62%			*OA*	93.15%	
	Kappa	0.8884			*Kappa*	0.8963	

According to Figure 8, the overall difference in the extraction results of the spatial distribution of mangroves for each vegetation index was not obvious, although the difference

was relatively obvious in the case of certain areas, as shown in the partially enlarged area in Figure 8. As shown in the figure, in cases where the tide level was high, it was likely that the $IMII_2$, *NDVI*, and *NDWI* classified other vegetation as mangroves, while the extraction results of the $IMII_1$, *SMRI*, and *EVI* were relatively accurate with relatively few errors.

According to Table 11, in study area C, there were only minor differences among the results when using different vegetation indexes to determine the spatial distribution of mangroves; the overall accuracy was higher than 92.6%, and the *Kappa* coefficient was greater than 0.88. In this case, the overall accuracy and *Kappa* coefficient of $IMII_2$ were the highest, with 93.97% and 0.91, respectively. The results of the *NDVI* were the lowest, with 92.62% and 0.89, respectively. The difference in overall accuracy and *Kappa* coefficient between $IMII_2$ and *NDVI* was only 1.35% and 0.02, respectively.

Meanwhile, it can be observed that various vegetation indices exhibited high mapping accuracy but low user accuracy in mangrove extraction, indicating a significant amount of misclassifications in the spatial distribution of mangroves using these indices. Among them, $IMII_2$ had the smallest difference between user accuracy and mapping accuracy, with only 3.55%, while *NDVI* had the largest difference, reaching 7.01%. This was primarily due to the complexity of tree species and the scattered distribution of mangroves in the study area, as well as the presence of a certain amount of *Spartina alterniflora* Loisel. invasion, resulting in many other vegetation types being misclassified as mangroves. The specific results are shown in the magnified area of Figure 8.

Similar to study areas A and B, the spatial distribution of mangroves was extracted using multivariate collaboration in study area C, and the results are shown in Table 12. And the confusion matrices of land cover classification with some vegetation indices based on Sentinel-2 images in study area C can be found in Table S3 in the Supplementary Materials.

Table 12. Partial multivariate combination classification results.

Multivariable Combination	Classification Results			Multivariable Combination	Classification Results		
		PA	*UA*			*PA*	*UA*
$IMII_1$, NDWI	Mangrove	95.67%	89.64%	***$IMII_2$, NDWI***	Mangrove	95.31%	92.53%
	Non-Mangrove	92.34%	95.15%		Non-Mangrove	93.78%	95.21%
	OA	93.07%			*OA*	94.08%	
	Kappa	0.8951			*Kappa*	0.9103	
		PA	*UA*			*PA*	*UA*
SMRI, NDVI	Mangrove	95.43%	88.22%	***EVI, NDVI***	Mangrove	95.43%	88.22%
	Non-Mangrove	91.91%	95.01%		Non-Mangrove	91.91%	95.01%
	OA	92.55%			*OA*	92.55%	
	Kappa	0.8873			*Kappa*	0.8873	
		PA	*UA*			*PA*	*UA*
$IMII_1$, NDWI, NDVI	Mangrove	95.31%	91.57%	***SMRI, NDWI, NDVI***	Mangrove	95.31%	90.73%
	Non-Mangrove	93.18%	95.01%		Non-Mangrove	92.88%	94.90%
	OA	93.63%			*OA*	93.33%	
	Kappa	0.9035			*Kappa*	0.8991	

Because of the complexity of the environment in study area C, most multivariate collaborative applications can improve classification results, as shown in Table 12. However, when *NDVI* was combined with other vegetation indices, the classification results may slightly decrease, such as *SMRI* and *NDVI*, as well as *EVI* and *NDVI* combinations.

In summary, the extraction results of the spatial distribution of mangroves of each vegetation index based on the medium-resolution Sentinel-2 images were not significantly different on the whole. However, the differences were relatively large in some regions, and the results of $IMII_2$ were relatively more accurate in comparison to the other vegetation indexes. This was mainly because the spatial resolution of Sentinel-2 images was relatively coarse, and the optimal resolution was only 10 m. Generally, for most areas, the longi-

tudinal length between the start and end lines of mangrove inundation rarely exceeded 10 m. Therefore, the difference between the extraction results of the spatial distribution of mangroves in most regions was less than one pixel, while the low mangroves in some regions became largely or even completely submerged during tidal inundation; this led to the occurrence of significant differences in the extraction results of the spatial distribution of mangroves. However, such regions were relatively small in the study area; thus, they did not lead to any significant differences in the overall extraction results of each vegetation index. At the same time, introducing different variables in SVM classification typically enhanced classification accuracy. This was because multivariable inputs provided more information and features, aiding in the accurate differentiation of various land cover categories. However, in some cases, the introduction of multiple variables may lead to a decrease in accuracy. This is because each variable provides features from a different perspective, which can introduce inconsistencies and uncertainty in the decision boundary of the algorithm.

4. Discussion

The accurate extraction of mangrove spatial distribution is the basis of mangrove dynamic change monitoring. However, due to the special growth area of mangroves, most of them grow in the coastal intertidal zone and are, therefore, affected by tidal inundation, mangroves in low positions will be completely submerged by high tide levels [14]. However, they will be exposed to the seawater at low tide level, resulting in inconsistent mangrove boundary information extracted from remote sensing image data at different tide levels. In theory, using images with lower tide levels can achieve more accurate extraction of mangrove spatial distribution. However, due to the transit time of satellites, tidal changes, and the influence of clouds and rain, it is often difficult to obtain images at the lowest or highest tide level. Most of the images obtained are from images between the highest and lowest tide levels, with mangroves located at low altitudes being more or less submerged, making it difficult to accurately extract the spatial distribution of mangroves. How to minimize the impact of tidal inundation based on most non-lowest level images is the foundation for achieving accurate extraction of mangrove spatial distribution. The collaborative application of high tide level images and nearest low tide level images provides new ideas and methods for eliminating the impact of tidal inundation on the spatial distribution of mangroves and achieving accurate extraction of submerged mangroves [22,25]. In this study, the *IMII*s were extracted based on high tide level images and nearest low tide level images and used to extract the spatial distribution of mangroves. The results showed that the extraction results of submerged mangroves based on *IMII*s were superior to those of commonly used vegetation indices and other vegetation index extracted based on high and low tide level images. This was mainly because compared to the vegetation index previously proposed based on high and low tide level images, *IMII*s integrated all four bands of red, green, blue, and near-infrared into the calculation formula of *IMII*s. However, the previous vegetation index only used a few bands without considering the four bands of red, green, blue, and near-infrared. From the results shown in Figure 3, it can be seen that there were differences in the spectral reflectance characteristics of tidal inundated mangroves and other land cover types among the four bands of the GF-2 image. Therefore, the collaborative application of the four bands can more comprehensively utilize the differences in spectral reflectance characteristics of different bands. At the same time, different algorithms such as addition, subtraction, multiplication, and division were comprehensively applied in the calculation formula of *IMII*s, which also amplified the differences in spectral reflectance characteristics to a certain extent, Ultimately, *IMII*s can achieve accurate extraction of mangroves. Although the study results indicated that *IMII*s can extract the spatial distribution of tidal inundated mangroves and verified its applicability on medium resolution Sentinel-2 images, there were still some shortcomings in extracting mangroves completely submerged by tides. This was mainly because the spectral reflectance characteristics of mangroves completely submerged by tides were very

similar to those of seawater, and relying solely on the red, green, blue, and near-infrared bands of high-resolution images was difficult to accurately distinguish between the spectral reflectance characteristics of submerged mangroves and seawater. Therefore, in the future, efforts can be made to collaborate with other data to extract the spatial distribution of mangroves under completely submerged tides.

In addition to the differences in bands and structures used in vegetation indices, sample selection is also an important factor affecting the classification results of mangroves [37]. The samples used in this study were mainly from Google Earth high-resolution images, the 2018 China mangrove resource distribution dataset, and field survey data. There was time difference between Google Earth high-resolution images, the China mangrove resource distribution dataset, and the GF-2 and Sentinel-2 images used by the study. Although Google Earth high-resolution images and the 2018 China mangrove resource distribution dataset were used for sample data mutual verification and proofreading when the sample data were selected and the vast majority of erroneous sample data were removed, it cannot be guaranteed that the sample points used were 100% correct due to the lack of field validation of these sample data. Meanwhile, due to the fact that most of the submerged mangroves were located in relatively distant offshore areas and the inability to conduct field investigations, the sample data of submerged mangroves selected based on Google Earth high-resolution images and the 2018 China mangrove resource distribution dataset may have contained some samples of *Spartina alterniflora* Loisel. The uncertainty in sample data can also have a certain impact on the extraction results of mangrove spatial distribution.

Several studies successfully extracted the spatial distribution of mangroves using different vegetation indices [38,39]; however, few studies verified the applicability of the proposed vegetation index on remote sensing images with other resolutions. In this study, in order to verify the applicability of a vegetation extraction index based on high-resolution images to other medium-resolution images, the *IMII*s, *SMRI*, *EVI*, *NDVI*, and *NDWI* were tested on Sentinel-2 images in three different regions. The results indicate that for Sentinel-2 images, the overall results of the extraction of the spatial distribution of mangroves with each vegetation index only contain minor differences; however, the results were relatively different in the case of other specific areas. This was primarily due to the fact that the height of mangrove trees in most of the selected three research areas was higher than the maximum tidal level; thus, the impact of tidal inundation was relatively small in these areas. Meanwhile, in most areas, the longitudinal length between the start and end lines of mangrove inundation was less than 10 m, while the optimal spatial resolution of Sentinel-2 images was 10 m, which made it difficult to achieve a complete pixel in the longitudinal direction of tidal inundation. The difference between the effects of tidal inundations on the spatial distribution of mangroves was less than one pixel; thus, the spatial distribution results of mangroves extracted by employing different vegetation indexes were not significantly different. However, in some specific areas, the mangrove tree species were complex and scattered, the tree height was relatively low, and the impact of tidal inundation was relatively large. Furthermore, there was a certain amount of *Spartina alterniflora* Loisel. invasion in some areas; as a result, some vegetation indices were unable to identify mangroves submerged by tides, and they may also mistakenly include *Spartina alterniflora* Loisel. in mangroves. The *IMII*, based on the high and low tide level images, was capable of identifying the mangroves submerged by the tide somewhat accurately and did not often misclassify *Spartina alterniflora* Loisel. as mangrove trees. Therefore, the overall extraction results of the spatial distribution of mangroves were not different in this case, but the differences were relatively large in the case of certain specific regions.

5. Conclusions

To eliminate the impact of tidal inundation on the extraction of spatial distribution of mangroves, the new vegetation indices, *IMII*s, were proposed based on GF-2 images of high and low tide levels. Meanwhile, other commonly used vegetation indices were also extracted. All the vegetation indices were used to extract the spatial distribution of

mangroves under tidal inundation, and applicability tests of the vegetation indices were conducted on Sentinel-2 images in three different regions. It was that a vegetation index that can accurately extract the spatial distribution of mangroves under tidal inundation in both medium and high-resolution images would be found. The main conclusions are as follows:

(1) The *IMII*s proposed based on GF-2 images of high and low tide levels can better identify mangroves inundated by tides, with results superior to those obtained from *SMRI*, *EVI*, *NDVI*, and *NDWI*. Among them, $IMII_2$ had the highest accuracy, followed by $IMII_1$, and *NDVI* had the lowest result.

(2) The proposed *IMII*s based on GF-2 images of high and low tide levels exhibited a favorable generalization applicability on Sentinel-2 images. The results of *IMII*s were relatively good among all vegetation indices, and the differences in the extraction results of different vegetation indices were obvious in areas with a significant impact of tidal inundation.

(3) In most cases, multi variables collaborative application can improve the accuracy of mangrove spatial distribution extraction results. For GF-2 images, the results of $IMII_1$, *NDVI*, and *NDWI* were relatively better among the three variable combinations, while for the two variable combinations, the results of $IMII_1$ and *NDWI* were relatively better.

Supplementary Materials: The following supporting information can be downloaded at: https://www.mdpi.com/article/10.3390/f14061145/s1, Figure S1: High resolution image from Google Earth in study area A on 14 October 2019; Figure S2: High resolution image from Google Earth in study area B on 15 September 2020; Figure S3: High resolution image from Google Earth in study area C on 5 November 2019; Figure S4: High resolution image from Google Earth in study area D on 21 February 2021; Table S1: The confusion matrices of land cover classification with some vegetation indices based on the GF-2 images; Table S2: The confusion matrices of land cover classification with some vegetation indices based on Sentinel-2 images in study area A; Table S3: The confusion matrices of land cover classification with some vegetation indices based on Sentinel-2 images in study area B; Table S4: The confusion matrices of land cover classification with some vegetation indices based on Sentinel-2 images in study area C.

Author Contributions: Conceptualization, H.Y. and F.W.; data curation, Q.Y., H.Y. and X.T.; formal analysis, Q.Y. and H.Y.; methodology, Q.Y., F.W. and Y.L.; supervision, J.C.; validation, F.W.; writing—original draft preparation, Q.Y. and H.Y.; writing—review and editing, J.C. and Q.Y. All authors have read and agreed to the published version of the manuscript.

Funding: This study was supported by grants from the National Natural Science Foundation of China (41901370,42261063), the Guangxi Natural Science Foundation (2020GXNSFBA297096), the Guangxi Science and Technology Base and Talent Project (GuikeAD19110064), and the BaGuiScholars program of the provincial government of Guangxi (Hongchang He).

Data Availability Statement: Not applicable.

Acknowledgments: We thank Guangxi Zhuang Autonomous Region Natural Resources Remote Sensing Institute for providing GF-2 images.

Conflicts of Interest: The authors declare no conflict of interest.

References

1. Saenger, P. Introduction: The Mangrove Environment. In *Mangrove Ecology, Silviculture and Conservation*; Springer: Dordrecht, The Netherlands, 2002; pp. 1–10.
2. Alongi, D.M. Mangrove forests: Resilience, protection from tsunamis, and responses to global climate change. *Estuar. Coast. Shelf Sci.* **2008**, *76*, 1–13. [CrossRef]
3. Kuenzer, C.; Bluemel, A.; Gebhardt, S.; Quoc, T.V.; Dech, S. Remote Sensing of Mangrove Ecosystems: A Review. *Remote Sens.* **2011**, *3*, 878–928. [CrossRef]
4. Brander, L.M.; Wagtendonk, A.J.; Hussain, S.S.; McVittie, A.; Verburg, P.H.; de Groot, R.S.; van der Ploeg, S. Ecosystem service values for mangroves in Southeast Asia: A meta-analysis and value transfer application. *Ecosyst. Serv.* **2012**, *1*, 62–69. [CrossRef]
5. Hussain, S.A.; Badola, R. Valuing mangrove benefits: Contribution of mangrove forests to local livelihoods in Bhitarkanika Conservation Area, East Coast of India. *Wetl. Ecol. Manag.* **2010**, *18*, 321–331. [CrossRef]
6. Danielsen, F. The Asian Tsunami: A Protective Role for Coastal Vegetation. *Science* **2005**, *310*, 643. [CrossRef]

7. Mazda, Y.; Magi, M.; Ikeda, Y.; Kurokawa, T.; Asano, T. Wave reduction in a mangrove forest dominated by *Sonneratia* sp. *Wetl. Ecol. Manag.* **2006**, *14*, 365–378. [CrossRef]
8. Donato, D.C.; Kauffman, J.B.; Murdiyarso, D.; Kurnianto, S.; Stidham, M.; Kanninen, M. Mangroves among the most carbon-rich forests in the tropics. *Nat. Geosci.* **2011**, *4*, 293–297. [CrossRef]
9. Lewis, M.; Pryor, R.; Wilking, L. Fate and effects of anthropogenic chemicals in mangrove ecosystems: A review. *Environ. Pollut.* **2011**, *159*, 2328–2346. [CrossRef]
10. Shapiro, A.; Trettin, C.; Küchly, H.; Alavinapanah, S.; Bandeira, S. The Mangroves of the Zambezi Delta: Increase in Extent Observed via Satellite from 1994 to 2013. *Remote Sens.* **2015**, *7*, 16504–16518. [CrossRef]
11. Wei, Z.; Zhenghua, C.; Jikun, W. Monitoring the areal variation of mangrove in Beibu Gulf coast of Guangxi China with remote sensing data. *J. Guangxi Univ. (Nat. Sci. Ed.)* **2015**, *40*, 1570–1576.
12. Mukhopadhyay, A.; Mondal, P.; Barik, J.; Chowdhury, S.M.; Ghosh, T.; Hazra, S. Changes in mangrove species assemblages and future prediction of the Bangladesh Sundarbans using Markov chain model and cellular automata. *Environ. Sci. Process. Impacts* **2015**, *17*, 1111. [CrossRef] [PubMed]
13. Zhenchao, Z.; He, L.; Chong, H.; Qingsheng, L.; Gaohuan, L.; Yun, H.; Han, Y. Review on dynamic monitoring of mangrove forestry using remote sensing. *J. Geo-Inf. Sci.* **2018**, *20*, 1631–1643. (In Chinese)
14. Giri, C.; Ochieng, E.; Tieszen, L.L.; Zhu, Z.; Singh, A.; Loveland, T.; Masek, J.; Duke, N. Status and distribution of mangrove forests of the world using earth observation satellite data. *Glob. Ecol. Biogeogr.* **2011**, *20*, 154–159. [CrossRef]
15. Lorenzo, E.N.; Jesus, B.D.; Jara, R.S. Assessment of mangrove forest deterioration in Zamboanga Peninsula, Philippines using LANDSAT MSS data. In Proceedings of the Thirteenth International Symposium on Remote Sensing of Environment, Environmental Research Institute of Michigan, Ann Arbor, MI, USA, 23–27 April 1979.
16. Lingyun, C.; Zining, H.; Shiquan, Z.; Wen, L.; Jianlong, S. Applying the Remote Sensing Information to Analyze Guangxi Mangrove Development Variety Characteristic. *Guangxi Sci.* **2005**, *12*, 308–311. (In Chinese)
17. Chungan, L.; Huabing, D. Extraction of Mangroves Spatial Distribution Using Remotely Sensed Data. *Wetl. Sci.* **2014**, *12*, 10. (In Chinese)
18. Kumar, T.; Mandal, A.; Dutta, D.; Nagaraja, R.; Dadhwal, V.K. Discrimination and classification of mangrove forests using EO-1 Hyperion data: A case study of Indian Sundarbans. *Geocarto Int.* **2019**, *34*, 415–442. [CrossRef]
19. Mingming, J.; Zongming, W.; Yuanzhi, Z.; Dehua, M.; Chao, W. Monitoring loss and recovery of mangrove forests during 42 years: The achievements of mangrove conservation in China. *Int. J. Appl. Earth Obs. Geoinf.* **2018**, *73*, 535–545.
20. Mingming, J.; Zongming, W.; Chao, W.; Dehua, M.; Yuanzhi, Z. A New Vegetation Index to Detect Periodically Submerged Mangrove Forest Using Single-Tide Sentinel-2 Imagery. *Remote Sens.* **2019**, *11*, 2043.
21. Xuehong, Z.; Jie, Z.; Yuanyuan, W.; Ye, Z. Remote sensing identification of mangrove forest combined tidal level information. *J. Nanjing Univ. Inf. Sci. Technol. (Nat. Sci. Ed.)* **2013**, *5*, 501–507. (In Chinese)
22. Xuehong, Z.; Qingjiu, T. A mangrove recognition index for remote sensing of mangrove forest from space. *Curr. Sci.* **2013**, *105*, 1149–1154.
23. Mingming, J. *Remote Sensing Analysis of China's Mangrove Forests Dynamics during 1973 to 2013*; Northeast Institute of Geography and Agroecology, Chinese Academy of Sciences: Changchun, China, 2014. (In Chinese)
24. Fang, X.; Ying, Z.; Liang, Z.; Jia, L.; Xianghui, G. Extraction method of intertidal mangrove by using Sentinel-2 images. *Bull. Surv. Mapp.* **2020**, *2*, 49–54. (In Chinese)
25. Qing, X.; Cheng Zhi, Q.; He, L.; Chong, H.; Fen Zhen, S. Mapping Mangrove Forests Based on Multi-Tidal High-Resolution Satellite Imagery. *Remote Sens.* **2018**, *10*, 1343.
26. Qing, X.; Jianhua, L.; Shuo, D.; Han, Z.; Qiong, Z.; Xuemin, X. Mapping high-resolution mangrove forests in China using remotely-sensed imagery under the tide. *Natl. Remote Sens. Bull.* **2022**. (In Chinese) [CrossRef]
27. Dezhi, W.; Bo, W.; Penghua, Q.; Yanjun, S.; Qinghua, G.; Run, W.; Fei, S.; Xincai, X. Evaluating the Performance of Sentinel-2, Landsat 8 and Pléiades-1 in Mapping Mangrove Extent and Species. *Remote Sens.* **2018**, *10*, 1468.
28. Gang, Y.; Ke, H.; Weiwei, S.; Xiangchao, M.; Dehua, M.; Yong, G. Enhanced mangrove vegetation index based on hyperspectral images for mapping mangrove. *ISPRS J. Photogramm. Remote Sens.* **2022**, *189*, 236–254.
29. Huete, A.R. Remote Sensing for Environmental Monitoring. *ScienceDirect* **2004**, *3*, 183–206.
30. Rouse, J.W.; Haas, R.H.; Schell, J.A.; Deering, D.W. Monitoring Vegetation Systems in the Great Plains with Erts. In *Third ERTS Symposium*; NASASP-351 I: Greenbelt, MD, USA, 1973; pp. 309–317.
31. Huete, A.; Didan, K.; Miura, T.; Rodriguez, E.P.; Gao, X.; Ferreira, L.G. Overview of the radiometric and biophysical performance of the MODIS vegetation indices. *Remote Sens. Environ.* **2002**, *83*, 195–213. [CrossRef]
32. Gao, B.C. *NDWI?*A Normalized Difference Water Index for Remote Sensing of Vegetation Liquid Water from Space. *Remote Sens. Environ.* **1996**, *58*, 257–266. [CrossRef]
33. Gupta, K.; Mukhopadhyay, A.; Giri, S.; Chanda, A.; Datta Majumdar, S.; Samanta, S.; Mitra, D.; Samal, R.N.; Pattnaik, A.K.; Hazra, S. An index for discrimination of mangroves from non-mangroves using LANDSAT 8 OLI imagery. *MethodsX* **2018**, *5*, 1129–1139. [CrossRef]
34. Vapnik, V. *Statistical Learning Theory New York*; Wiley: New York, NY, USA, 1998.
35. Zhihua, Z. Machine Learning. *Chin. Civ. Commer.* **2016**, *3*, 93. (In Chinese)
36. Hang, L. *Statistical Learning Methods*; Tsinghua University Press: Beijing, China, 2012. (In Chinese)

37. Shahriar, S.H.; Giorgos, M. Effect of classifier selection, reference sample size, reference class distribution and scene heterogeneity in per-pixel classification accuracy using 26 Landsat sites. *Remote Sens. Environ.* **2018**, *204*, 648–658.
38. Tiezhu, S.; Jue, L.; Zhongwen, H.; Huizeng, L.; Junjie, W.; Guofeng, W. New spectral metrics for mangrove forest identification. *Remote Sens. Lett.* **2016**, *7*, 885–894.
39. Norida, M.; Chinsu, L. Exploring changes of land use and mangrove distribution in the economic area of Sidoarjo District, East Java using multi-temporal Landsat images. *Inf. Process. Agric.* **2017**, *4*, 321–332.